

Manganese Complex of a Rigidified 15-Membered Macrocyclic: A Comprehensive Study

Kristof Pota, Enikő Molnár, Ferenc Krisztián Kálmán, David M. Freire, Gyula Tircsó,* and Kayla N. Green*



Cite This: <https://dx.doi.org/10.1021/acs.inorgchem.0c01053>



Read Online

ACCESS |



Metrics & More

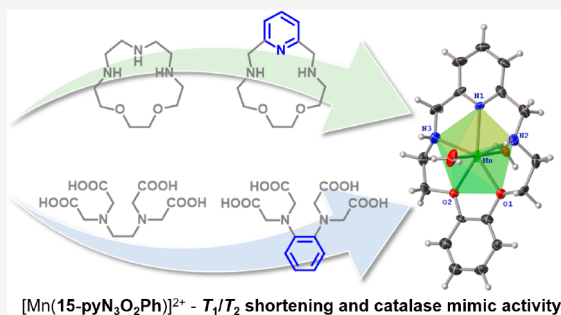


Article Recommendations



Supporting Information

ABSTRACT: Owing to the increasing importance of manganese(II) complexes in the field of magnetic resonance imaging (MRI), large efforts have been devoted to find an appropriate ligand for Mn(II) ion encapsulation by providing balance between the seemingly contradictory requirements (i.e., thermodynamic stability and kinetic inertness vs low ligand denticity enabling water molecule(s) to be coordinated in its metal center). Among these ligands, a large number of pyridine or pyridol based open-chain and macrocyclic chelators have been investigated so far. As a next step in the development of these chelators, 15-pyN₃O₂Ph and its transition metal complexes were synthesized and characterized using established methods. The 15-pyN₃O₂Ph ligand incorporates both pyridine and *ortho*-phenylene units to decrease ligand flexibility. The thermodynamic properties, protonation and stability constants, were determined using pH-potentiometry; the solid-state structures of the free ligand and its manganese complex were obtained by single crystal X-ray diffractometry. The results show a seven-coordinate metal center with two water molecules in the first coordination sphere. The longitudinal relaxivity of [Mn(15-pyN₃O₂Ph)]²⁺ was found to be 5.16 mM⁻¹ s⁻¹ at 0.49 T (298 K). Furthermore, the *r*_{2p} value of 11.72 mM⁻¹ s⁻¹ (0.49 T), which is doubled at 1.41 T field, suggests that design of this Mn(II) complex does achieve some characteristics required for contrast imaging. In addition, ¹⁷O NMR measurements were performed in order to access the microscopic parameters governing this key feature (e.g., water exchange rate). Finally, manganese complexes of ligands with analogous polyaza macrocyclic scaffold have been investigated as low molecular weight Mn(CAT) mimics. Here, we report the H₂O₂ disproportionation study of [Mn(15-pyN₃O₂Ph)]²⁺ to demonstrate the versatility of this ligand scaffold as well.



INTRODUCTION

As first shown by Pedersen, 15-membered macrocycles containing five heteroatoms have the ability to function as complexing agents.¹ From this starting point, a large library of ligands bearing oxygen and nitrogen donor atoms have been synthesized and explored for a diverse field of applications.^{2–4} In these studies, crown- and aza-crown ethers have shown the capability to act as phase-transfer catalysts in organic reactions.^{5–8} Mn(II) complexes of these ligands are known as highly active and stable superoxide dismutase (MnSOD) or catalase (Mn(CAT)) mimics.^{9–11} Another promising application is the use of the high-spin Mn(II) chelates as magnetic resonance imaging (MRI) contrast agents (CAs).¹²

At present, about 40% of all MRI procedures use one of the seven Gd(III)-based contrast agents (GBCAs) that are commercially marketed and available in the U.S., Europe, or Japan to diagnose tissue and vascular abnormalities.¹³ However, it is important to note that the use of some of the agents containing a linear ligand are suspended or restricted in Europe, and warnings have been issued by the United States Food and Drug Administration (FDA) due to concerns about

potential free gadolinium toxicity.^{14–16} It is now proven that the injected dose is not completely excreted, which can lead to delayed toxicity. The first association between MRI agents and a disease was made in 2006, when patients with impaired renal function were diagnosed with nephrogenic systemic fibrosis (NSF).^{17,18} More recently, a series of reports revealed long-term gadolinium retention in the central nervous system in the case of patients without renal impairment.¹⁹

Manganese complexes have been proposed as possible alternatives for the GBCAs. The d⁵ Mn(II) ion is a very effective relaxation agent due to its preference for a high-spin (*S* = 5/2) electron configuration and a characteristically long longitudinal electron spin relaxation time.²⁰ However, the coordination number is limited to six or seven in aqueous

Received: April 9, 2020

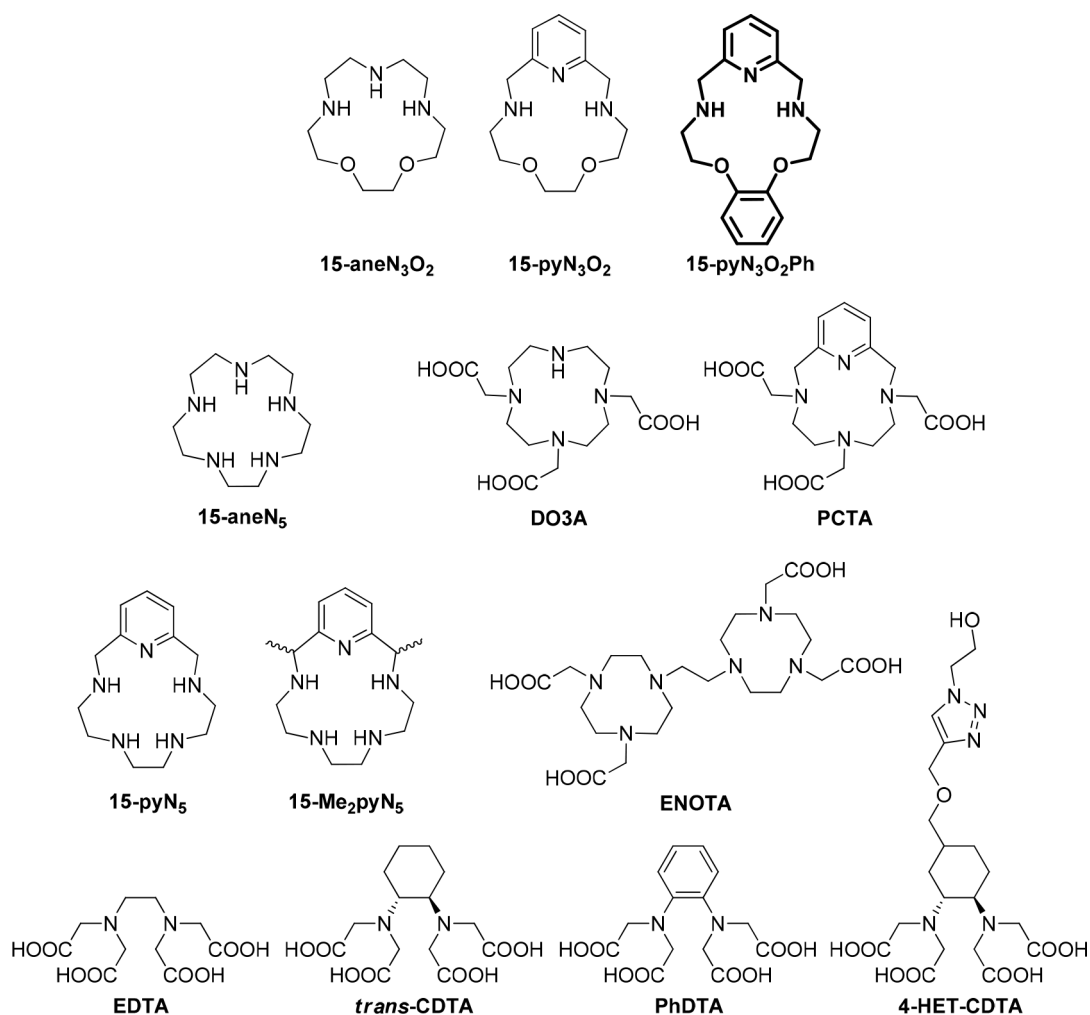


Figure 1. Structure of ligands studied or discussed in the present work.

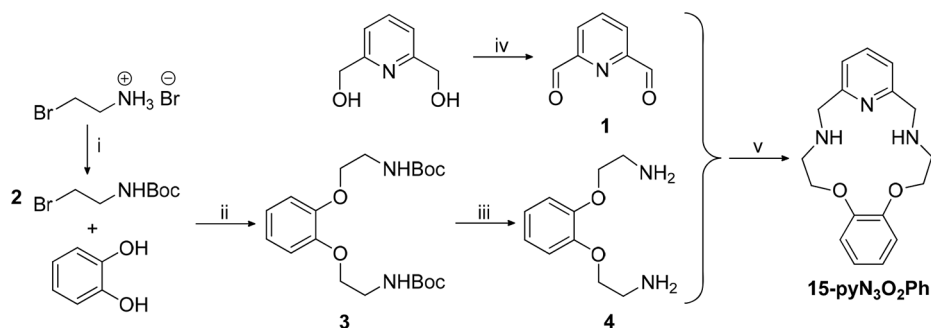
chelates with Mn(II), compared to the Gd(III) coordination number of nine, a typical value for later lanthanide metal ions. For the targeted imaging activity, the Mn(II) complexes must accommodate at least one water molecule in the first coordination sphere. Hence, hexadentate, open-chain ligands garnered increased interest in recent years as a means of replacing GBCAs.^{21,22}

Several studies have shown that ligand rigidity may be a key feature to maintain an intact complex upon injection for imaging *in vivo*.^{22–25} It was shown that the rigidification of the backbone leads to a 150–250 fold increase in the kinetic inertness of the Mn(II) complexes of the *trans*-CDTA and PhDTA ligands compared to the EDTA congener (Figure 1).^{21,26} Inclusion of a pyridine moiety into a macrocycle is an alternative approach to increase the resistance of these chelates toward proton assisted dissociation. It was shown that the dissociation half-life of the [Mn(PCTA)][−] complex (pH = 7.4) is more than 5 times higher compared to the [Mn(DO3A)][−].²⁷ The validity of this second method has already been successfully reported for 15-membered pentaaza-macrocycles: the [Mn(15-pyN₅)]²⁺ complex should remain intact during the course of an MRI experiment under physiological conditions.¹²

On the basis of these reports, we set out to further decrease the flexibility of pentadentate chelators using the 15-membered macrocyclic base structure (15-aneN₃O₂) with the inclusion of both the pyridine (15-pyN₃O₂) and the *ortho*-phenylene units.

Accordingly, the objective of the study was to synthesize and characterize the 15-pyN₃O₂Ph ligand and its transition metal complexes, with an emphasis on the Mn(II) complex (Figure 1). Here, we report the synthesis and crystal structures of the free ligand and its manganese bound form. The thermodynamic properties, protonation, and stability constants of 15-pyN₃O₂Ph and several of its alkaline-earth and transition metal complexes were determined by pH-potentiometric titrations using 0.15 M NaCl ionic strength to model physiological conditions. Furthermore, relaxation properties of the complex formed with Mn(II) were studied by ¹H relaxometry, while ¹⁷O NMR studies were used to gain information about the exchange rate of the metal ion bound solvent molecules.

Manganese complexes of 15-membered pentaaza-crown ether macrocycles have also been extensively explored as mimics for metalloenzymes with a particular focus on catalase reactivity.¹¹ Catalase enzymes are essential for living cells to protect them against oxidative stress. Their main function is to catalyze the disproportionation of a toxic oxygen metabolite, hydrogen peroxide (H₂O₂), into molecular oxygen (O₂) and water (H₂O) before it is transformed into reactive oxygen species (ROS) like the hydroxyl radical (OH•) through other redox pathways.²⁸ Most catalase enzymes are composed of an iron-protoporphyrin IX prosthetic group, but some living organisms utilize manganese based enzymes (e.g., Mn(CAT)) instead. Ligand features modulate the stability and activity of

Scheme 1. Synthesis of 15-pyN₃O₂Ph^a

^aConditions: (i) Boc₂O, Et₃N, CH₂Cl₂, RT, 18 h. (ii) K₂CO₃, MeCN, reflux, 24 h. (iii) Step 1: AcCl, MeOH, RT, 24 h. Step 2: NaOH(s), MeCN. (iv) MnO₂, CHCl₃, reflux, 5 h. (v) Step 1: MnCl₂, MeOH, reflux, 2 h. Step 2: NaBH₄, RT, 14 h. Step 3: H₂O on air, RT, 1 h.

the manganese center toward hydrogen peroxide disproportionation; in particular aza-oxa-macrocyclic complexes of manganese have been studied as Mn(CAT) models due to their high formation constants. Structural changes in the substituents of the macrocycle seem to have an effect in both the kinetic of the reaction and mechanism pathway, although the latter is still unclear.¹¹ The [Mn(15-pyN₃O₂Ph)]²⁺ complex was found to catalyze the disproportionation of H₂O₂. To quantify its activity, a series of experiments was conducted under controlled conditions.

EXPERIMENTAL SECTION

General. The pyridine-2,6-dicarbaldehyde (1),^{12,29–31} *tert*-butyl-(2-bromoethyl)carbamate (2),³² di-*tert*-butyl-([1,2-phenylenebis(oxy)]bis[ethane-2,1-diyl])dicarbamate (3),³³ and 2,2'-[1,2-phenylenebis(oxy)]diethanamine (4),³⁴ Scheme 1) were prepared according to literature procedures (or slightly modified, see Supporting Information). Methanol was distilled from KOH and stored over 4 Å molecular sieves. Other solvents and chemicals were purchased from commercial sources and used as received. NMR spectra were recorded on a Bruker Avance III 400 MHz High Performance Digital NMR Spectrometer at 298 K: ¹H (400.1 MHz), TMS (internal): δ 0.00 ppm; ¹³C (100.6 MHz), TMS (internal): δ 0.00 ppm. Multiplicity of the signals is indicated as follows: s, singlet; d, doublet; t, triplet; q, quartet; m, multiplet; br, broad. Deuterated solvents (Aldrich: CDCl₃, 99.8% D; Cambridge Isotope Laboratories: CD₃OD, 99.8% D; DMSO-*d*₆, 99.96% D) were used as received. Mass spectra were obtained on an Agilent 1200 series 6224 TOF LC/MS spectrometer equipped with an electro-spray ion source at 75 V (positive ion mode).

Synthesis of Cyclo(2,6-pyridinediylmethyleneiminoethyle-noxy-1,2-phenyleneoxyethyleneiminomethylene) (15-py-N₃O₂Ph). Compound 4 (0.476 g, 3.52 mmol) and MnCl₂·4H₂O (0.697 g, 3.52 mmol) were dissolved in dry MeOH (50 mL). A solution of 1 (0.691 g, 3.52 mmol) in dry MeOH (30 mL) was added dropwise over 15 min. The reaction mixture was refluxed for 2 h. After cooling to 0 °C, NaBH₄ (1.81 g, 47.8 mmol) was added in small portions. The solution was left stirring overnight at RT. Water (40 mL) was slowly added, which induced the precipitation of Mn(OH)₂ and immediate oxidation. The resulting suspension was stirred at RT for 1 h. MeOH was removed *in vacuo*, and the remaining aqueous phase was filtered on a frit under a vacuum. The brown precipitate, which formed upon quenching, was washed with CH₂Cl₂ (3 × 40 mL), and the aqueous phase was extracted with the CH₂Cl₂. The organic layer was dried with anhydrous Na₂SO₄, and the solvent was evaporated under reduced pressure. The crude product was purified by column chromatography (SiO₂, EtOH/cc-NH₃(aq.) = 100:1) and dried *in vacuo* at 50 °C. Yield: 0.342 g (33%), light yellow solid, R_f = 0.43 (EtOH/cc-NH₃(aq.) = 100:1). ¹H NMR (400 MHz, CDCl₃): δ 7.56 (t, J = 7.6 Hz, 1H), 7.05 (d, J = 7.6 Hz, 2H), 6.90 (s, 4H), 4.16 (t, J = 4.8 Hz, 4H), 3.95 (s, 4H), 3.05 (t, J = 4.8 Hz, 4H). ¹³C NMR

(100.6 MHz, CDCl₃): δ 158.4, 149.0, 136.7, 121.1, 120.4, 113.3, 68.4, 53.9, 49.0. HRMS (ESI, *m/z*) calcd for C₁₇H₂₂N₃O₂ [M + H]⁺: 300.1712. Found: 300.1901; calcd for C₁₇H₂₁N₃NaO₂ [M + Na]⁺: 322.1531. Found: 322.1585. Elemental analysis for 2C₁₇H₂₁N₃O₂·2C₂H₅OH·HCl found (calcd): C, 62.23 (62.75); H, 7.40 (7.62); N, 11.47 (11.55).

Crystal Structure Determination. Single crystals of 15-pyN₃O₂Ph were obtained by slow evaporation of a CH₃OH solution. Low quality single crystals of the perchlorate salt of 15-pyN₃O₂Ph were obtained by slow evaporation of the aqueous ligand solution, which was acidified by two drops of perchloric acid (70%). The manganese complex solution was prepared by mixing the aqueous solutions of the ligand (*c*_L = 17 mM) and manganese(II) chloride (*c*_{Mn} = 50 mM) in a Mn/L molar ratio of 1:1.02. The solution was evaporated under reduced pressure, and the residue was dissolved in EtOH and filtered through a syringe filter (0.45 μm PTFE membrane). Colorless single crystals suitable for the X-ray diffraction analysis were prepared by slow evaporation of the EtOH solution at room temperature.

A Leica MZ 75 microscope was used to identify samples suitable for analysis. A Bruker APEX-II CCD diffractometer was employed for crystal screening, unit cell determination, and data collection, which were obtained at 100 K. The Bruker D8 goniometer was controlled using the APEX3 software suite.³⁵ The samples were optically centered with the aid of a video camera so that no translations were observed as the crystal was rotated through all positions. The X-ray radiation employed was generated from a Mo Kα sealed X-ray tube (λ = 0.71076 Å) with a potential of 50 kV and a current of 30 mA, fitted with a graphite monochromator in the parallel mode (175 mm collimator with 0.5 mm pinholes).

Potentiometric Measurements. The MgCl₂, CaCl₂, MnCl₂, FeCl₃, CuCl₂, and ZnCl₂ stock solutions were prepared from analytical grade chemicals, and their concentrations were determined by complexometric titrations with standardized Na₂H₂EDTA and an eriochrome black-T (EBT) indicator for MgCl₂ and CaCl₂, EBT indicator in the presence of ascorbic acid and triethanol-amine for MnCl₂, thiosalicylic acid indicator in the presence of ascorbic acid and pyridine for FeCl₃, PAR indicator in the presence of NH₄OAc for CuCl₂, and EBT indicator in the presence pH 10 NH₃/NH₄Cl buffer for ZnCl₂. The concentration of the ligand stock solution was determined by pH-potentiometric titration. The protonation constants were calculated with the following setup: 0.2 M carbonate free NaOH titrant with 2 mM ligand solution at an initial volume of 6 mL. Titrations were performed at 25.0 ± 0.1 °C and an ionic strength of *I* = 0.15 M NaCl to model the background present in body fluids. An inert atmosphere was provided by a constant passage of dry N₂ through the sample. The protonation constants of the ligand (log *K*_i^H) are defined as

$$K_i^H = \frac{[H_iL^{i+}]}{[H_{i-1}L^{(i-1)+}][H^+]} \quad (1)$$

where $i = 1, 2,$ and 3 and $[H_{i-1}L^{(i-1)+}]$ and $[H^+]$ are the equilibrium concentrations of the ligand in different protonation states and hydrogen ions, respectively. The potentiometric titrations were carried out with a Metrohm 785 DMP Titrino workstation and a Metrohm 6.0234.100 combined electrode in the pH range of 2.0–11.8. For the calibration of the microelectrode, KH-phthalate (pH = 4.008)³⁶ and borate (pH = 9.177)³⁷ buffer standards were used, and the $[H^+]$ were calculated from the measured pH values by applying the method proposed by Irving et al.³⁸ A solution of approximately 0.01 M HCl was titrated with 0.2 M NaOH solution ($I = 0.15$ M NaCl), and the differences between the measured and calculated pH values (pH < 2.2) were used to calculate the $[H^+]$ from the pH values measured in the ligand titrations. The experimental points above pH 11 for the acid–base titration were utilized to determine the ionic product of water (13.840) in case of our experimental setup. PSEQUAD software was used to calculate the equilibrium constants.³⁹ The protonation constants of the 15-pyN₃O₂Ph ligand were determined by titrating the ligand solution (acidified with a known volume of standard HCl solution) with 0.2 M NaOH at 0.15 M NaCl ionic strength in the 2.0–11.8 pH range. The log K_i^H values were calculated from 150 V (mL)–pH data pairs. To determine the stability constants of the complexes formed with different metal ions, potentiometric titrations were carried out at a 1:1 metal-to-ligand molar ratio, with 2% ligand excess to prevent the hydrolysis of the metal ions, allowing 1 min for the equilibration to occur (the number of data pairs were between 70 and 160).

¹H-Relaxometric Studies. Measurements of longitudinal (T_1) and transverse (T_2) relaxation times were performed by using Bruker Minispec MQ-20 and MQ-60 NMR Analyzers working at 0.49 T (corresponding to 20 MHz proton Larmor frequency) and 1.41 T (corresponding to 60 MHz proton Larmor frequency), respectively. The temperature of the sample holder was set (25.0 ± 0.2 °C) and controlled with the use of a circulating water bath. The T_1 values were determined with the inversion recovery method ($180_x^\circ - \tau - 90_x^\circ$) by averaging four to six data points obtained at 10 different τ delay values. The transverse relaxation times (T_2) were measured by using the Carr–Purcell–Meiboom–Gill sequence (CPMG) by averaging again four to six identical data points.⁴⁰ The r_{1p} and r_{2p} relaxivities of the complex were determined by using batch samples (lying in the concentration range of 0.5–2.0 mM) prepared under a nitrogen atmosphere having the ligand present at a 1.8-fold excess in the presence of 5 equiv of a hydroxyl-amine reducing agent (to prevent the oxidation of the Mn(II)). The pH in these samples was kept constant at pH = 8.14 with the use of HEPES buffer ($I = 0.15$ M NaCl, $T = 298$ K). By relying on the species distribution curves under these conditions, only one Mn(II) ion containing species is present in solution, which is the $[Mn(15\text{-pyN}_3\text{O}_2\text{Ph})]^{2+}$ complex. To confirm the complex formation and its pH range, a sample containing 1 mM of the ligand and Mn(II) ($V_{\text{tot}} = 6$ mL) was titrated with NaOH under a N₂ protected atmosphere, and the $1/T_{1,2p}$ data were collected in the pH range of 4.5–11.0.

¹⁷O NMR Studies. Longitudinal ($1/T_1$) and transverse ($1/T_2$) relaxation rates and chemical shifts of an aqueous solution of the Mn(II) complex (pH = 8.14, at 1.9 mM concentration) and of a diamagnetic reference (HClO₄ acidified water, pH = 3.3) were measured in the temperature range 273–348 K using a Bruker Avance 400 (9.4 T, 54.2 MHz) spectrometer. Analogously to the ¹H relaxometric measurements, the ligand was used in a 100% excess compared to Mn(II) to limit the free metal ion concentration. In order to avoid the oxidation of the Mn(II) ion in the complex, hydroxyl-amine was added to the sample (at 5 mM concentration), based on accepted protocols. The temperature was determined according to previous calibration routines by means of ethylene glycol as a standard.⁴¹ $1/T_1$ and $1/T_2$ values were determined by the inversion–recovery and the Carr–Purcell–Meiboom–Gill spin–echo technique, respectively.⁴⁰ The ¹⁷O NMR technique for accessing water exchange rates has been described previously.⁴² To avoid susceptibility corrections of the chemical shifts, a glass sphere fitted into a 10 mm NMR tube was used during the measurements. To increase the sensitivity of ¹⁷O NMR measurements, ¹⁷O enriched

water (10% H₂¹⁷O, NUKEM Isotopes Imaging GmbH) was added to the solutions to reach a 2% enrichment. The fit of the ¹⁷O NMR data was performed using Micromath Scientist calculation program via least-squares fitting procedure.

Reaction of Mn(II) Complex with H₂O₂ and Quantification of O₂ Evolution. The reactions were performed in a sealed pressure vessel (15 mL) equipped with a stirring bar and a three-way manifold valve. Two of the lines (PTFE tubing) were connected to the cell: one was used for N₂ and the other to inject the aliquot of H₂O₂. The pressure vessel was sealed using a PEEK bushing connected to threaded fittings (IDEX Health and Science) for custom sealing between the gas tubing, microsensor and reaction vessel. The pressure of the vessel was kept at 1 atm using a snorkel line with minimal loss of headspace during the catalytic studies. The sensor was calibrated using N₂ and air (0 and 159 mmHg) under atmospheric pressure.

The metal complex was prepared in aqueous solution at pH = 8 using stock solutions of 15-pyN₃O₂Ph, buffer, and MnCl₂. At pH 8, 95% of the Mn(II) ions are chelated by the ligand. Tris-(hydroxymethyl)aminomethane buffer was used to maintain the desired pH during the experiments. The metal complex was prepared by mixing the corresponding amount of the stock solution of ligand, buffer, and MnCl₂ in a vial to achieve the targeted concentration for the H₂O₂ disproportionation studies ($[15\text{-pyN}_3\text{O}_2\text{Ph}] = 2.04$ mM; $[\text{buffer}] = 50$ mM; $[\text{Mn(II)}] = 2$ mM). The vessel was loaded with 1.5 mL of the catalyst and pressurized with N₂ gas prior to every measurement. The electrode signal was read continuously and measured every 0.2 s until a steady signal was obtained for 2 min, then 0.5 mL of H₂O₂ solution was injected ($[\text{H}_2\text{O}_2] = 600$ mM, $[\text{buffer}] = 50$ mM). The signal was recorded as ΔP_{O_2} vs time until a plateau was achieved. The initial concentrations of the species before starting the reaction were $[15\text{-pyN}_3\text{O}_2\text{Ph}] = 1.54$ mM, $[\text{Mn(II)}] = 1.5$ mM, and $[\text{H}_2\text{O}_2] = 150$ mM.

RESULTS AND DISCUSSION

Synthesis. The synthesis of 15-pyN₃O₂Ph was achieved by convergent pathways (Scheme 1). The pyridine containing unit of 15-pyN₃O₂Ph, pyridine-2,6-dicarbaldehyde (**1**), was prepared from the commercially available 2,6-bis-(hydroxymethyl)pyridine through partial oxidation of the hydroxyl groups with MnO₂ according to literature procedures.^{12,29–31} The other half of the macrocycle was prepared in a three step synthesis, which started with the protection of the amine functional group of commercially available 2-bromoethylamine as the carbamate. The Boc protecting group was chosen because of its increased resistance to basic and nucleophile reagents as well as its ease of removal with close to quantitative yields.³⁴ The reagent ratio was modified in the case of the amine protection to remove the excess Boc₂O from the reaction mixture. The alkylation of the catechol was based on the literature procedure.³³ The workup of this reaction was modified, and as a result, we were able to separate the pure mono- and bis-alkylated products utilizing the difference between their solubility in water at different pH values. The deprotection step was achieved with excellent yield (94%), but the free base form of the amine was necessary for the cyclization, which led to a slightly decreased yield of 78%. Mn(II) ions were used for cyclization of **1** and **4** in a one-pot template synthesis; the reaction conditions to prepare the intermediate Schiff-base and subsequent reduction paralleled those described in previously published procedures for other triaza-dioxa macrocyclic systems (Scheme 1).^{12,43} The final product was obtained in a 33% overall yield as a light-yellow solid after purification by column chromatography, and connectivity was confirmed by ¹H and ¹³C NMR, MS, and elemental analysis.

Solid State Structures: Crystal Structure of the Ligand. Two different protonation states of the 15-pyN₃O₂Ph ligand were characterized by single crystal X-ray diffractometry. The base form ([15-pyN₃O₂Ph]⁰, Figure 2) possesses a near

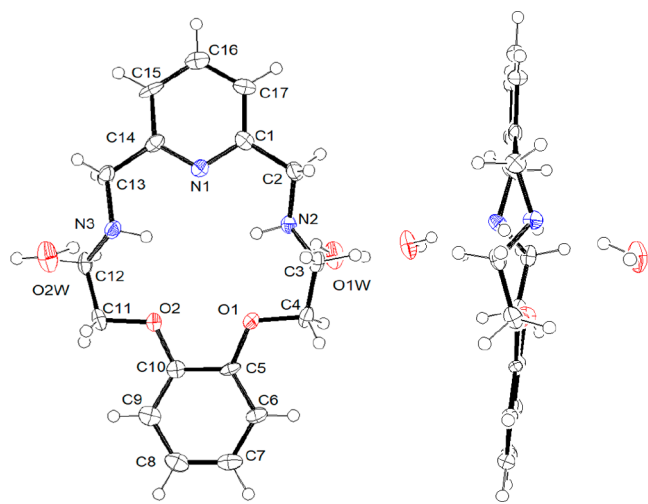


Figure 2. Molecular structure of 15-pyN₃O₂Ph (front and side view). The thermal ellipsoids are drawn with 50% probability.

planar structure with a pseudo-C₂ symmetry axis passing through carbon C16, nitrogen N1, and the center of the benzene ring (bonds C5–C10, C7–C8). A similar but more emphasized symmetry element can be observed in the acid form (propeller like twist, best visualized from the top view, [H₃(15-pyN₃O₂Ph)]³⁺, Figure 3), which is analogous to the structure of the parent molecule ([H₃(15-pyN₃O₂)]³⁺).¹² The proton on the pyridine nitrogen atom (N1) is hydrogen bonding with oxygen atoms O1 and O2 resulting in $d_{N-O} \sim 2.8$ Å, which represent a drastic shrink in the macrocyclic cavity compared to the base form, where the same distances are around 4.2 Å. This structural change can help explain the observed nearly instantaneous dissociation of the Mn(II) complex upon acidification.

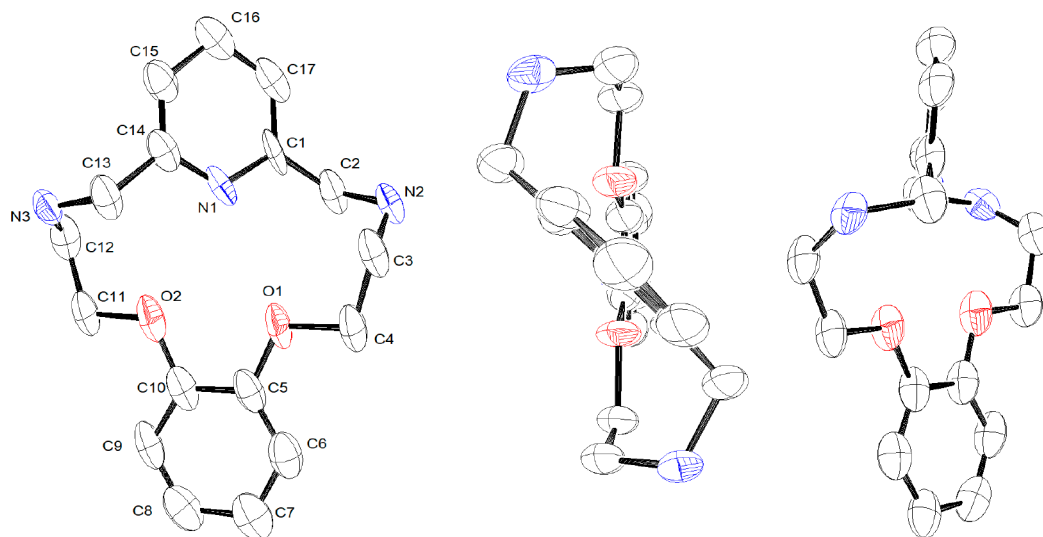


Figure 3. Molecular structure of [H₃(15-pyN₃O₂Ph)]³⁺ (front, top, and side view). Hydrogen atoms, solvent molecules, and counterions are omitted for clarity. The thermal ellipsoids are drawn with 50% probability.

Solid State Structure of the Mn(II) Complex. The manganese complex was prepared by the addition of MnCl₂ to an aqueous solution of 15-pyN₃O₂Ph. Materials suitable for X-ray diffraction analysis were obtained by evaporating MeOH solutions of the crude product. The solid state model has a composition of [Mn(15-pyN₃O₂Ph)(H₂O)₂]Cl₂; a Mn(II) ion can be found in the center of the planar macrocyclic cavity with three nitrogen and two oxygen atoms in the equatorial plane and two water molecules in the apical positions forming the pentagonal-bipyramidal coordination sphere (Figure 4). A

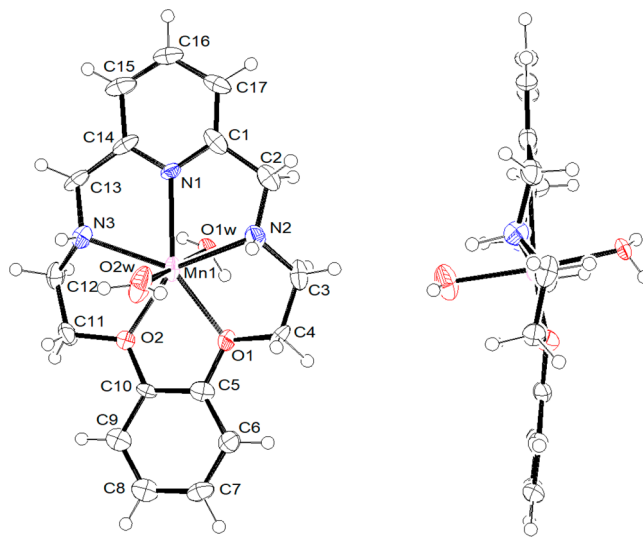


Figure 4. Molecular structure of the [Mn(15-pyN₃O₂Ph)(H₂O)₂]²⁺ unit (front and side view). The thermal ellipsoids are drawn with 50% probability.

seven coordinate Mn(II) ion has been observed with aminopolycarboxylate ligands like EDTA, but this is only the second reported crystal structure with two water molecules in the first coordination sphere with a pentadentate macrocycle.^{44,45} The Mn(II) complex of 15-pyN₃O₂ and 15-pyN₅ had two chlorides or one chloride and one water molecule, respectively.¹² Of course, these chlorides are replaced by water molecules in

aqueous solution based on the ^{17}O NMR experiments described below. The previously mentioned π - π stacking of the pyridine and phenylene moieties can be observed in the unit cell of the manganese complex, similarly to the free base form of the ligand. The only major difference is that the C_2 symmetry of the free base form was lost because the metal center forced the two secondary amines to reside on the same side of the plane determined by the pyridine ring (Figures 2 and 3). Four out of the five chelate rings in the complex have alternating δ/λ conformations starting from the pyridine nitrogen atom ($\delta\lambda$ - $\delta\lambda$). The only exception is the five-membered ring opposite the pyridine, which is planar due to structural requirements of the phenylene group. All coordination bonds are within the expected range and are consistent with those reported in related structures (Table 1).^{10,12,45-47}

Table 1. Selected Interatomic Distances (Å) Found in the Crystal Structure of $[\text{Mn}(15\text{-pyN}_3\text{O}_2\text{Ph})(\text{H}_2\text{O})_2]\text{Cl}_2$ Compared to Representative Examples of Mn(II)-Complexes with Pentadentate Macrocycles

	$[\text{Mn}(15\text{-aneN}_3\text{O}_2)\text{Cl}_2]^{\text{a}}$	$[\text{Mn}(15\text{-Me}_2\text{pyN}_3\text{O}_2)(\text{H}_2\text{O})_2]^{\text{2+,b}}$	$[\text{Mn}(15\text{-pyN}_3\text{O}_2)(\text{H}_2\text{O})\text{Cl}]^{\text{+,c}}$	$[\text{Mn}(15\text{-pyN}_3\text{O}_2\text{Ph})(\text{H}_2\text{O})_2]^{\text{2+,d}}$
Mn-N1	2.26	2.278	2.229	2.340(4)
Mn-N2	2.41	2.343	2.334	2.346(4)
Mn-N3	2.45	2.352	2.300	2.339(4)
Mn-O1			2.250	2.167(3)
Mn-O2			2.305	2.208(3)
Mn-O1w		2.282	2.230	2.207(13)
Mn-O2w		2.241		2.141(16)

^aRef 46. ^bRef 45. ^cRef 12.

The Mn-N distances (2.34–2.35 Å) of $[\text{Mn}(15\text{-pyN}_3\text{O}_2\text{Ph})(\text{H}_2\text{O})_2]\text{Cl}_2$ are slightly longer than the Mn-O bonds (2.14–2.21 Å) with either the oxygen atoms in the macrocycle or the water molecules. The bond angles between the neighboring donor atoms of the macrocycle and the central Mn(II) ion range from 70.6 to 74.5°, which is consistent with the theoretical value of 72° of the regular pentagon. Also, the regular *trans*-apical coordination is confirmed by the bond angle of 174.9° between the water molecules and the divalent center (Table S5). The Mn-O distance for the coordinated water molecules is slightly shorter than in complexes with similar pentadentate macrocycles (Table 1). A possible explanation for this result might be the increased planarity of the ligand, which is induced by the two aromatic systems on the opposite sides of the structure.

Equilibrium Studies. Stepwise protonation constants of 15-pyN₃O₂Ph as well as stability constants of its complexes with various alkaline earth and transition metal ions were determined by standard pH-potentiometric titrations (Tables 2

Table 2. Stepwise Protonation Constants of 15-Membered Triaza-Dioxa Macrocycles ($T = 298\text{ K}$, $I = 0.15\text{ M NaCl}$)

	15-aneN ₃ O ₂	15-pyN ₃ O ₂ ^c	15-pyN ₃ O ₂ Ph
$\log K_1^{\text{H}}$	9.29, ^a 9.51 ^b	8.82	8.53(3)
$\log K_2^{\text{H}}$	8.50, ^a 8.47 ^b	7.80	7.63(3)
$\log K_3^{\text{H}}$	2.12, ^a 2.30 ^b		
$\Sigma \log K_i^{\text{H}}$	19.91, ^a 20.28 ^b	16.62	16.16

^aRef 48 ($I = 0.1\text{ M NaNO}_3$). ^bRef 49 ($I = 0.1\text{ M KNO}_3$). ^cRef 12 ($I = 0.1\text{ M Me}_4\text{NCl}$).

and 3). For these experiments, 0.15 M NaCl ionic strength was used to model the conditions present in bodily fluids. Two

Table 3. Stability Constants ($\log K$) of Complexes Formed with Divalent Metal Ions and 15-Membered Triaza-Dioxa Macrocycles ($T = 298\text{ K}$, $I = 0.15\text{ M NaCl}$, Charges in the Equilibrium Quotients Were Omitted for Clarity)

	equilibrium quotient	15-aneN ₃ O ₂	15-pyN ₃ O ₂ ^d	15-pyN ₃ O ₂ Ph
Mg(II)	$[\text{ML}]/([\text{M}][\text{L}])$ $[\text{ML}]/([\text{M}(\text{OH})\text{L}][\text{H}])$			1.84(9)
Ca(II)	$[\text{ML}]/([\text{M}][\text{L}])$ $[\text{ML}]/([\text{M}(\text{OH})\text{L}][\text{H}])$		2.04 11.92	1.85(8)
Mn(II)	$[\text{ML}]/([\text{M}][\text{L}])$ $[\text{ML}]/([\text{M}(\text{OH})\text{L}][\text{H}])$	6.63 ^a	7.18 11.69	5.62(3) 10.50(4)
Fe(II)	$[\text{ML}]/([\text{M}][\text{L}])$ $[\text{ML}]/([\text{M}(\text{OH})\text{L}][\text{H}])$	7.79 ^a 9.1 ^a		7.35(3) 10.78(5)
Co(II)	$[\text{ML}]/([\text{M}][\text{L}])$ $[\text{ML}]/([\text{M}(\text{OH})\text{L}][\text{H}])$	8.49 ^a	9.48 11.80	7.65(4)
Cu(II)	$[\text{ML}]/([\text{M}][\text{L}])$ $[\text{ML}]/([\text{M}(\text{OH})\text{L}][\text{H}])$	15.72, ^a 15.27 ^b 8.87, ^a - ^b	13.91 8.34	13.97(2) 8.95(6)
	$[\text{M}(\text{OH})\text{L}]/([\text{M}(\text{OH})_2\text{L}][\text{H}])$		12.57	
Zn(II)	$[\text{ML}]/([\text{M}][\text{L}])$ $[\text{ML}]/([\text{M}(\text{OH})\text{L}][\text{H}])$	8.95, ^a 8.85, ^b 8.91 ^c -, ^{a,b} 8.85 ^c	8.58	7.70(3) 9.62(5)

^aRef 49 ($I = \text{M KNO}_3$). ^bRef 48 ($I = 0.1\text{ M NaNO}_3$). ^cRef 51 ($I = 0.1\text{ M NaCl}$). ^dRef 12 ($I = 0.1\text{ M Me}_4\text{NCl}$).

protonation events were found for 15-pyN₃O₂Ph that are attributed to subsequent protonation of the secondary amine nitrogen atoms. However, protonation of the pyridine nitrogen atom is outside of the limits of our experimental conditions. These results are in good agreement with previously reported values for 15-membered triaza-dioxa macrocycles.^{12,48,49} Comparison of the stepwise $\log K_i^{\text{H}}$ values (Table 2) shows that, with the introduction of the pyridine moiety, the basicity of the adjacent secondary amine nitrogen atoms decreased only slightly (approximately 0.5 log units) due to the electron-withdrawing effect of the aromatic system compared to 15-aneN₃O₂. However, the total basicity decreased noticeably because of the replacement of the amine nitrogen atoms with a pyridine unit. On the other hand, only negligible attenuation of the $\log K_i^{\text{H}}$ values and the basicity of the ligand are observed between 15-pyN₃O₂ and 15-pyN₃O₂Ph after the introduction of the phenylene group on the opposite side of the molecule. This difference is attributed to the electron withdrawing nature of the phenylene group compared to ethylene. The species distribution diagram for the 15-pyN₃O₂Ph can be found in the Supporting Information (Figure S17).

The values of the stability constants for the complexes of 15-pyN₃O₂Ph with a range of divalent alkaline-earth and first-row transition metal ions (Table 3) were determined using the same conditions as for the ligand titrations. The results show that 1:1 complexes form for each of the systems studied. The stability of the ternary hydroxo chelates could be calculated for almost all metal ions. The Irving-Williams' order of stability is

followed for all the transition metal ions with a maximum value for the Cu(II) complex.⁵⁰

A few important conclusions can be drawn from the comparison of the formation constants for the three 15-membered aza-oxa macrocycles (Figure 5). First, the effect of

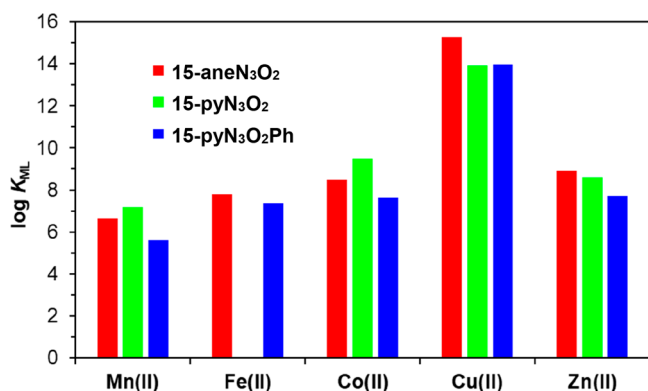


Figure 5. Transition metal complex stabilities of the discussed ligands.

the pyridine moiety (15-pyN₃O₂) on the stability of Mn(II) and Co(II) complexes is overturned with the introduction of the second aromatic system to the macrocyclic framework (15-pyN₃O₂Ph). The respective constants are 1.56 and 1.83 log units lower for the chelates formed with 15-pyN₃O₂Ph. This behavior is most likely due to the highly increased rigidity of the ligand, which causes a decrease in the entropy component of the binding configurational entropy of the ligand. However, in case of the Cu(II) binding affinity this structural modification is not present, the value describing the strength of interaction is almost within the error of the experimental technique (for the species distribution diagram, see Figure S18). Unfortunately, the rather small stability constant for the Mn(II) complex means that even by pH 8, only 95% of the cation is chelated by the macrocycle (Figure S19). Therefore, the addition of the phenylene moiety has decreased the formation stability of the Mn(II) outside of the window of applicability for imaging studies, thus it represents a stopping point for consideration in future ligand design.

¹H-Relaxometric Studies. Complex formation involving paramagnetic metal ions can be studied through ¹H relaxometric method by following the longitudinal (*T*₁) or transverse (*T*₂) relaxation times (or *r*_{1p} and *r*_{2p} relaxivities) as a function of pH. The data obtained by the given technique might provide supporting data to the equilibrium model established (often set by the expert) for the fitting of the pH-potentiometric data by comparing the species distribution curves calculated using stability constants determined by pH-potentiometry with the pH profile of the relaxivity. Such a profile was first obtained for a sample containing equimolar amounts of the metal ion and the ligand (Figure S19). While the given profile confirmed the complex formation in the Mn(II)–15-pyN₃O₂Ph–H⁺ system, formation of the precipitate near pH = 9.5 (corresponding to the precipitation of uncomplexed Mn(II)) narrows the pH-range available for the study. Thus, we performed a titration of the sample with an excess of the ligand to push the reaction toward full complexation. Hydroxyl-amine was added to the sample in parallel to overcome the oxidation of Mn(II). The normalized relaxivities and molar fraction of the species present in solution was calculated by using the pH-potentiometric measurements

plotted together as a function of pH in the graph depicted in Figure 6. The comparison of the curves indicates that the

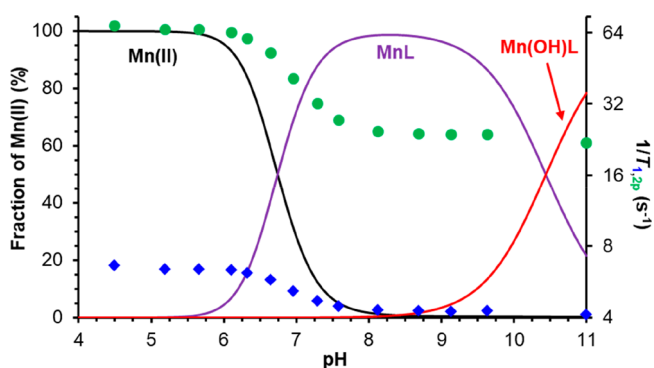


Figure 6. Species distribution diagram of the complex [Mn(15-pyN₃O₂Ph)]²⁺ calculated in the pH range of 4 to 11 (by using 1.0 mM of Mn(II) and 2.0 mM ligand; solid lines) and the plots of the 1/*T*_{1p} (blue diamonds) and 1/*T*_{2p} (green circles) values measured at 1.41 T and 0.15 M NaCl at 298 K (charges are omitted for clarity).

equilibrium model applied for the fitting of pH-potentiometric data describes the complex formation correctly. Formation of [Mn(15-pyN₃O₂Ph)]²⁺ starts only at pH 5.70, and it reaches a maximum only near pH 8.0, even with ligand excess applied. However, raising the pH above 9.0 results in the formation of ternary hydroxo species. These results are consistent with the formation of a relatively weak Mn(II) complex with the 15-pyN₃O₂Ph ligand, partially due to an excess of ligand rigidity.

On the basis of the information presented in Figure 6, the relaxivity of the [Mn(15-pyN₃O₂Ph)]²⁺ complex was determined by plotting the 1/*T*_{1p} values of samples as a function of complex concentration (Figure S20) at pH 8.14 (set by HEPES buffer). The relaxivity values were compared to data measured for structurally similar systems under the same conditions (Table 4). The relaxivity of the [Mn(15-pyN₃O₂Ph)]²⁺ complex (5.16 mM⁻¹ s⁻¹ at 0.49 T (298 K)) is in the same range as those determined for 15-pyN_xO_{5-x} derivatives.¹² This value is in agreement with the presence of more than one water molecule in the inner sphere of the Mn(II) center, which was validated by ¹⁷O NMR following the method proposed by Gale et al., as expected based on an

Table 4. Relaxivities and Best Fit Parameters Obtained from the Analysis of ¹⁷O NMR Data for the Mn(II) Complexes of 15-pyN₃O₂Ph, 15-pyN₃O₂, 15-pyN₅, ENOTA, and 4-HET-CDTA

parameter	15-pyN ₃ O ₂ Ph	15-pyN ₃ O ₂ ^a	15-pyN ₅ ^a	ENOTA ^b	4-HET-CDTA ^c
<i>r</i> _{1p} / <i>r</i> _{2p} (mM ⁻¹ s ⁻¹) at 0.49 T (298 K) ^d	5.16/11.72	4.48/–	3.56/–	3.39/–	4.87/–
<i>k</i> _{ex} ²⁹⁸ (10 ⁷ s ⁻¹)	0.64 ± 0.05	0.38	6.9	5.5	17.6
Δ <i>H</i> [‡] (kJ mol ⁻¹)	34 ± 3	35.3	37.7	20.5	36.2
Δ <i>S</i> [‡] (J mol ⁻¹ K ⁻¹)	–1 ± 10	–1	+32	–28	+34
<i>A</i> ₀ / <i>η</i> (10 ⁶ rad s ⁻¹)	43 ± 14	38.6	38.6	32.7	40 ^e
1/ <i>T</i> _{1s} ²⁹⁸ (10 ⁷ s ⁻¹)	11 ± 8				7

^aRef 12. ^bRef 56. ^cRef 57. ^d*r*_{1p} and *r*_{2p} are 4.49 and 25.69 mM⁻¹ s⁻¹ at 1.41 T (298 K).

analogy of the Mn(II) complexes formed with the parent 15-pyN₃ and 15-pyN₃O₂ chelators.⁵² The relaxivity of [Mn(15-pyN₃O₂Ph)]²⁺ is larger than those reported for the FDA-approved Gd(III)-based contrast agents (for example, Dotarem in water, $r_{1p} = 3.4 \text{ mM}^{-1} \text{ s}^{-1}$ at 0.49 T (313 K) and $2.9 \text{ mM}^{-1} \text{ s}^{-1}$ at 1.41 T (310 K)).⁵³ It should also be noted that the [Mn(15-pyN₃O₂Ph)]²⁺ complex possesses a r_{2p} value of $11.72 \text{ mM}^{-1} \text{ s}^{-1}$ (0.49 T), which is doubled at a 1.41 T field, suggesting that [Mn(15-pyN₃O₂Ph)]²⁺ can be an efficient T_2 shortening agent.

¹⁷O NMR Measurements. In order to gain information on the water exchange rate (k_{ex}) of the Mn(II) complex, one of the most important physicochemical parameters affecting the relaxivity of a paramagnetic metal complex, temperature dependent ¹⁷O NMR experiments were carried out. The transverse and longitudinal relaxation rates as well as the chemical shift of the ¹⁷O signal in the presence and absence of the paramagnetic agent can provide information on the k_{ex} , the rotational motion, and the electronic parameters, while the chemical shift is correlated to the number of the water molecules directly coordinated to the paramagnetic metal center (q). The relaxation rates ($1/T_1$ and $1/T_2$) and chemical shifts ($\Delta\omega_r$) were measured for an aqueous solution of [Mn(15-pyN₃O₂Ph)]²⁺ and for a diamagnetic reference at 9.4 T. The T_1 values showed a negligible difference between the Mn(II) complex and the reference and thus were not included in the calculations. The Swift–Connick equations were used, by assuming a simple exponential behavior for the electron spin relaxation, for the fitting of the $1/T_{2r}$ values and chemical shifts.^{54,55} The plots of the experimental data together with the fitted curves are depicted in Figure 7. The water exchange rate,

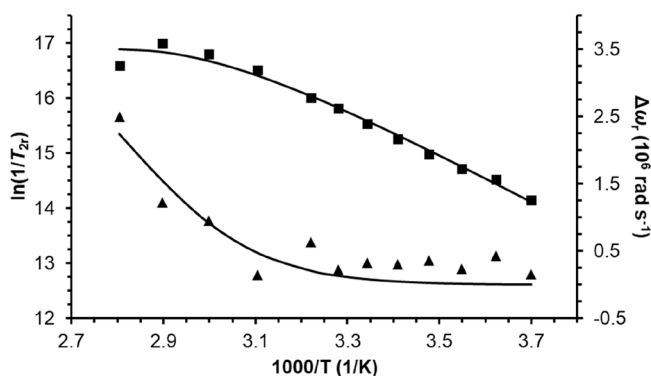


Figure 7. Reduced ¹⁷O transverse relaxation rates (squares) and chemical shifts (triangles) measured for the [Mn(15-pyN₃O₂Ph)]²⁺ complex ($c_{\text{Mn}^{2+}} = 1.90 \text{ mM}$ and $c_{\text{Lig}} = 3.80 \text{ mM}$ at pH = 8.14). The solid lines correspond to the best fit of the data.

k_{ex} ²⁹⁸, its activation enthalpy, ΔH^\ddagger , the hyperfine coupling constant, A_O/\hbar , and $1/T_{1e}^{298}$ were calculated (the activation energy of electron spin relaxation was fixed to 1 kJ/mol). The hydration number was set to $q = 2$ based on analogy to the results published by Drahos et al. for the complexes [Mn(15-pyN₃O₂Ph)]²⁺ and [Mn(15-pyN₃)]²⁺.¹² This assumption was confirmed by the transverse relaxation rates of the ¹⁷O nucleus in the presence of the paramagnetic Mn(II) complex ($q = 1.6 \pm 0.2$).⁵²

The reduced transverse ¹⁷O relaxation rates are in the slow water exchange regime at lower temperatures reaching a maximum at around 341 K (Figure S21). The k_{ex} value characterizing the water exchange of [Mn(15-pyN₃O₂Ph)]²⁺ is

ca. 50% higher than that of the [Mn(15-pyN₃O₂)]²⁺ complex and 1 order of magnitude lower than the value determined for the [Mn(15-pyN₃)]²⁺ chelate. Accepting the explanation given by Drahos et al., the strength of the hydrogen bond formed between the water proton and the O donors of the ligand affects the rate of the water exchange.¹² The incorporation of the phenyl group into the macrocyclic backbone increases the rigidity of the coordination cavity around the Mn(II) ion due to its planar structure, which in turn has a significant impact on the length and strength of the hydrogen bonds involving the coordinated water molecules. This might be one of the explanations for the decreased water exchange rate of the complex and is in agreement with the results obtained by X-ray crystallography, which indicates a slight shortening of the Mn–O_w bonds in [Mn(15-pyN₃O₂Ph)]²⁺ in comparison with [Mn(15-Me₂pyN₃(H₂O)₂]²⁺ and [Mn(15-pyN₃O₂)(H₂O)Cl]⁺.^{12,45} The activation entropy for [Mn(15-pyN₃O₂Ph)]²⁺ is close to zero ($\Delta S^\ddagger = -1 \pm 10 \text{ J mol}^{-1} \text{ K}^{-1}$), indicating that the water exchange very likely occurs via an interchange mechanism. The six-coordinated Mn(II) complexes frequently go through associatively activated water exchange, while the seven-coordinate chelates often show a dissociatively activated process.^{56,57} Similar behavior was observed for the [Mn(15-pyN₃O₂)]²⁺ complex as well.

Catalytic H₂O₂ Disproportionation. In order to investigate the effect of the 15-pyN₃O₂Ph ligand on this reactivity, H₂O₂ disproportionation reactions were carried out using a one-pot approach.⁵⁸ The pH of the solution was selected based on the speciation curve; at pH 8, 95% of the Mn(II) ions are chelated by the ligand (Figure S19). An O₂ microsensor probe (Unisense, Denmark) inserted into a sealed pressure vessel, previously flushed with N₂, was used to continuously measure the partial pressure of O₂ (P_{O_2}) in mmHg every 0.2 s. Addition of H₂O₂ resulted in oxygen evolution based on the formation of bubbles in the solution and a significant increase in P_{O_2} measured by the sensor. O₂ evolution plateaued at 60 min. Control reactions were carried out with either the ligand or the metal by itself, which showed a small O₂ evolution signal using the same conditions, validating the need for the metal complex in solution for catalysis to occur.

The results were plotted as ΔP_{O_2} (mmHg) vs time (min) (Figure 8). The O₂ pressure increased continuously after the

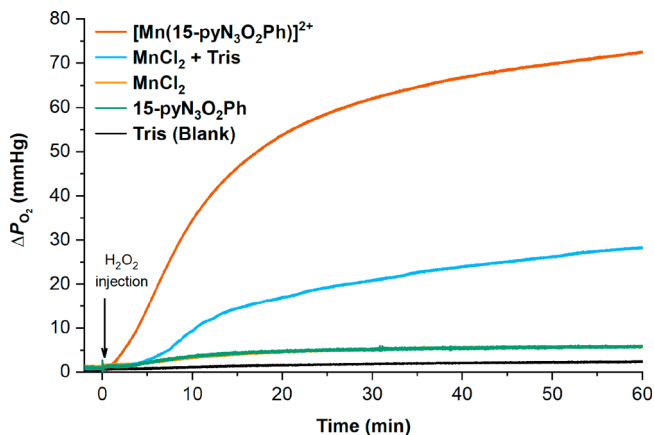


Figure 8. O₂ evolution from H₂O₂ disproportionation reaction catalyzed by [Mn(15-pyN₃O₂Ph)]²⁺. Initial conditions: [Mn(II)] = 1.5 mM, [H₂O₂] = 150 mM, [buffer] = 50 mM.

injection of H₂O₂. The turnover frequency (TOF) was calculated at different times from the injection of H₂O₂ at 1, 10, 20, and 60 min (Table 5). At 60 min, the TOF is lower

Table 5. ΔP_{O_2} , TON, and TOF Based on Oxygen Production from the Decomposition of H₂O₂ (150 mM) by Mn(II) Complex of 15-pyN₃O₂Ph

ΔP_{O_2} (mmHg)	TON	TOF (min ⁻¹)			
		1 min	10 min	20 min	60 min
67(4)	15(1)	0.4(1)	0.92(4)	0.61(7)	0.21(3)

than at 1 min, which indicates that a plateau has been reached. The turnover number (TON) was calculated for a reaction period of 60 min, since no significant increase of the signal was observed after this point.

Table 5 shows the ΔP_{O_2} for three different trials, turnover number (TON), and turnover frequencies at different times. Figure 8 shows the O₂ evolution signal measured by the O₂ microsensor probe. Both ΔP_{O_2} and TON were calculated at the end of a reaction period of 60 min, but a constant increase of the signal was observed, which could be attributed to the natural disproportionation of H₂O₂. To determine the rate of O₂ evolution for TOF calculations different slopes were calculated at several times (1, 10, 20, and 60 min); in the first minute, several bubbles form in the solution and slowly diffuse out of it, the rate keeps increasing for a few minutes and then starts to decrease at 60 min where the plateau is reached. After that, no more catalytic activity was observed. Overall, the results indicate that the complex is indeed a functional mimic of Mn(CAT) but has limited activity under the conditions studied.

CONCLUSIONS

In summary, we have shown that the inclusion of a second aromatic ring into the backbone of a 15-membered macrocyclic system leads to a formation of a surprisingly flat manganese(II) complex with two water molecules bound in the solid state. This structural feature plays a key role in increasing the longitudinal relaxivity (r_{1p}) of the chelate compared to its parent molecule, due to the open axial positions around the seven-coordinate metal center. It must be mentioned, that [Mn(15-pyN₃O₂Ph)]²⁺ has a transverse relaxivity of 11.72 mM⁻¹ s⁻¹ at 0.49 T (298 K), which is boosted to 25.69 mM⁻¹ s⁻¹ at 1.41 T (298 K), suggesting that the complex might act as an efficient T₂ shortening agent. These results are supported by a wide array of well-established experimental techniques (i.e., pH-potentiometric, XRD, ¹⁷O NMR and ¹H relaxometric measurements). Unfortunately, it has to be noted that as an adverse effect of rigidification, the Mn(II) chelate is unsuitable for further investigations as a contrast agent due to its labile nature under even mildly acidic conditions. However, we have also demonstrated its activity as an H₂O₂ disproportionation catalyst, which creates new opportunities for Mn(CAT) mimics with macrocyclic ligands.

ASSOCIATED CONTENT

Supporting Information

The Supporting Information is available free of charge at <https://pubs.acs.org/doi/10.1021/acs.inorgchem.0c01053>.

Details of synthesis, NMR spectra, crystallographic data, equilibrium and relaxometric studies, and details related to the ¹⁷O measurements (PDF)

Accession Codes

CCDC 1992320 and 1992322 contain the supplementary crystallographic data for this paper. These data can be obtained free of charge via www.ccdc.cam.ac.uk/data_request/cif, or by emailing data_request@ccdc.cam.ac.uk, or by contacting The Cambridge Crystallographic Data Centre, 12 Union Road, Cambridge CB2 1EZ, UK; fax: +44 1223 336033.

AUTHOR INFORMATION

Corresponding Authors

Kayla N. Green – Department of Chemistry and Biochemistry, Texas Christian University, Fort Worth, Texas 76129, United States; orcid.org/0000-0001-8816-7646; Email: kayla.green@tcu.edu

Gyula Tircsó – Department of Physical Chemistry, University of Debrecen, Debrecen, Hungary H-4032; orcid.org/0000-0002-7896-7890; Email: gyula.tircso@science.unideb.hu

Authors

Kristof Pota – Department of Chemistry and Biochemistry, Texas Christian University, Fort Worth, Texas 76129, United States; orcid.org/0000-0002-9027-0201

Enikő Molnár – Department of Physical Chemistry, University of Debrecen, Debrecen, Hungary H-4032

Ferenc Krisztián Kálmán – Department of Physical Chemistry, University of Debrecen, Debrecen, Hungary H-4032; orcid.org/0000-0001-9000-2779

David M. Freire – Department of Chemistry and Biochemistry, Texas Christian University, Fort Worth, Texas 76129, United States

Complete contact information is available at:

<https://pubs.acs.org/10.1021/acs.inorgchem.0c01053>

Notes

The authors declare no competing financial interest.

ACKNOWLEDGMENTS

K.P. is grateful for the support from the Fulbright Foundation and the College of Science and Engineering at TCU. This work was funded by the National Institutes of Health R15GM123463 (to K.N.G.). The authors are also grateful for generous financial support from TCU Andrews Institute of Mathematics and Science Education (to K.N.G.), Cambridge Isotope Laboratories, and TCU Research and Creativity Activity Grant (to K.N.G.). The authors (E.M., F.K.K., and G.T.) acknowledge financial support from the Hungarian National Research, Development and Innovation Office (NKFIH K-120224 project) and the COST Action CA15209 European Network on NMR Relaxometry. The research was also supported in a part by the EU and cofinanced by the European Regional Development Fund under the project GINOP-2.3.2-15-2016-00008.

REFERENCES

- Pedersen, C. J. Cyclic Polyethers and Their Complexes with Metal Salts. *J. Am. Chem. Soc.* **1967**, *89* (26), 7017–7036.
- Yoshio, M.; Noguchi, H. Crown Ethers for Chemical Analysis: A Review. *Anal. Lett.* **1982**, *15* (15), 1197–1276.
- Klok, H.-A.; Eibeck, P.; Schmid, M.; Abu-Surrah, A. S.; Möller, M.; Rieger, B. Novel Benzo-15-Crown-5 Functionalized α -Olefin/CO

- Terpolymers for Membrane Applications. *Macromol. Chem. Phys.* **1997**, *198* (9), 2759–2768.
- (4) Chen, C.-Y.; Cheng, C.-T.; Lai, C.-W.; Wu, P.-W.; Wu, K.-C.; Chou, P.-T.; Chou, Y.-H.; Chiu, H.-T. Potassium Ion Recognition by 15-Crown-5 Functionalized CdSe/ZnS Quantum Dots in H₂O. *Chem. Commun.* **2006**, No. 3, 263–265.
- (5) Tarnag, J.-Y.; Shih, J.-S. Crown Ether as the Phase-Transfer Catalyst for Free Radical Polymerization of Hydrophobic Vinyl Monomers. *J. Chin. Chem. Soc.* **1994**, *41* (1), 81–87.
- (6) Bako, P.; Rapi, Z.; Grun, A.; Nemcsok, T.; Hegedus, L.; Keglevich, G. Asymmetric Michael Addition of Malonates to Enones Catalyzed by an α -D-Glucopyranoside-Based Crown Ether. *Synlett* **2015**, *26* (13), 1847–1851.
- (7) Bardsley, K.; Hagigeorgiou, M.; Lengyel, I.; Cesare, V. New One-Step Synthesis of Isonitriles. *Synth. Commun.* **2013**, *43* (12), 1727–1733.
- (8) Nemcsok, T.; Rapi, Z.; Bagi, P.; Oláh, A.; Keglevich, G.; Bakó, P. The Synthesis of Hydrobenzoin-Based Monoaza Crown Ethers and Their Application as Recyclable Enantioselective Catalysts. *Catal. Lett.* **2020**, *150* (4), 930–938.
- (9) Harris, J. M.; Hundley, N. H.; Shannon, T. G.; Struck, E. C. Poly(ethylene glycols) as Soluble, Recoverable, Phase-Transfer Catalysts. *J. Org. Chem.* **1982**, *47* (24), 4789–4791.
- (10) Riley, D. P.; Lennon, P. J.; Neumann, W. L.; Weiss, R. H. Toward the Rational Design of Superoxide Dismutase Mimics: Mechanistic Studies for the Elucidation of Substituent Effects on the Catalytic Activity of Macrocyclic Manganese(II) Complexes. *J. Am. Chem. Soc.* **1997**, *119* (28), 6522–6528.
- (11) Signorella, S.; Palopoli, C.; Ledesma, G. Rationally Designed Mimics of Antioxidant Manganoenzymes: Role of Structural Features in the Quest for Catalysts with Catalase and Superoxide Dismutase Activity. *Coord. Chem. Rev.* **2018**, *365*, 75–102.
- (12) Drahos, B.; Kotek, J.; Hermann, P.; Lukes, I.; Toth, E. Mn²⁺ Complexes with Pyridine-Containing 15-Membered Macrocycles: Thermodynamic, Kinetic, Crystallographic, and ¹H/¹⁷O Relaxation Studies. *Inorg. Chem.* **2010**, *49* (7), 3224–3238.
- (13) *The Chemistry of Contrast Agents in Medical Magnetic Resonance Imaging*, 2nd ed.; Wiley, 2013.
- (14) Li, B.; Du, Y.; Wei, H.; Dong, S. Reusable, Label-Free Electrochemical Aptasensor for Sensitive Detection of Small Molecules. *Chem. Commun.* **2007**, *0* (36), 3780–3782.
- (15) Ren, J. M.; Trokowski, R.; Zhang, S. R.; Malloy, C. R.; Sherry, A. D. Imaging the Tissue Distribution of Glucose in Livers Using A PARACEST Sensor. *Magn. Reson. Med.* **2008**, *60* (5), 1047–1055.
- (16) Le Fur, M.; Caravan, P. The Biological Fate of Gadolinium-Based MRI Contrast Agents: A Call to Action for Bioinorganic Chemists. *Metallomics* **2019**, *11* (2), 240–254.
- (17) Marckmann, P.; Skov, L.; Rossen, K.; Dupont, A.; Damholt, M. B.; Heaf, J. G.; Thomsen, H. S. Nephrogenic Systemic Fibrosis: Suspected Causative Role of Gadodiamide Used for Contrast-Enhanced Magnetic Resonance Imaging. *J. Am. Soc. Nephrol.* **2006**, *17* (9), 2359–2362.
- (18) Grobner, T. Gadolinium – a specific trigger for the development of nephrogenic fibrosing dermopathy and nephrogenic systemic fibrosis? *Nephrol. Dial. Transplant.* **2006**, *21* (4), 1104–1108.
- (19) McDonald, R. J.; McDonald, J. S.; Kallmes, D. F.; Jentoft, M. E.; Murray, D. L.; Thielen, K. R.; Williamson, E. E.; Eckel, L. J. Intracranial Gadolinium Deposition after Contrast-enhanced MR Imaging. *Radiology* **2015**, *275* (3), 772–782.
- (20) Lauffer, R. B. Paramagnetic Metal Complexes as Water Proton Relaxation Agents for NMR Imaging: Theory and Design. *Chem. Rev.* **1987**, *87* (5), 901–927.
- (21) Pota, K.; Garda, Z.; Kalman, F. K.; Barriada, J. L.; Esteban-Gomez, D.; Platas-Iglesias, C.; Toth, I.; Brucher, E.; Tircso, G. Taking the Next Step Toward Inert Mn²⁺ Complexes of Open-Chain Ligands: The Case of the Rigid PhDTA Ligand. *New J. Chem.* **2018**, *42* (10), 8001–8011.
- (22) Gale, E. M.; Atanasova, I. P.; Blasi, F.; Ay, I.; Caravan, P. A Manganese Alternative to Gadolinium for MRI Contrast. *J. Am. Chem. Soc.* **2015**, *137* (49), 15548–57.
- (23) Wedeking, P.; Kumar, K.; Tweedle, M. F. Dissociation of Gadolinium Chelates in Mice: Relationship to Chemical Characteristics. *Magn. Reson. Imaging* **1992**, *10* (4), 641–648.
- (24) Puttagunta, N. R.; Gibby, W. A.; Smith, G. T. Human *in vivo* Comparative Study of Zinc and Copper Transmetallation after Administration of Magnetic Resonance Imaging Contrast Agents. *Invest. Radiol.* **1996**, *31* (12), 739–742.
- (25) Gibby, W. A.; Gibby, K. A.; Gibby, W. A. Comparison of Gd DTPA-BMA (Omniscan) versus Gd HP-DO3A (ProHance) Retention in Human Bone Tissue by Inductively Coupled Plasma Atomic Emission Spectroscopy. *Invest. Radiol.* **2004**, *39* (3), 138–142.
- (26) Kálmán, F. K.; Tircsó, G. Kinetic Inertness of the Mn²⁺ Complexes Formed with AAZTA and Some Open-Chain EDTA Derivatives. *Inorg. Chem.* **2012**, *51* (19), 10065–10067.
- (27) Garda, Z.; Molnár, E.; Kálmán, F. K.; Botár, R.; Nagy, V.; Baranyai, Z.; Brucher, E.; Kovács, Z.; Tóth, I.; Tircsó, G. Effect of the Nature of Donor Atoms on the Thermodynamic, Kinetic and Relaxation Properties of Mn(II) Complexes Formed With Some Trisubstituted 12-Membered Macrocyclic Ligands. *Front. Chem.* **2018**, *6*, 232/1–232/14.
- (28) Chelikani, P.; Fita, I.; Loewen, P. C. Diversity of structures and properties among catalases. *Cell. Mol. Life Sci.* **2004**, *61* (2), 192–208.
- (29) Papadopoulos, E. P.; Jarrar, A.; Issidorides, C. H. Oxidations with Manganese Dioxide. *J. Org. Chem.* **1966**, *31* (2), 615–616.
- (30) Vance, A. L.; Alcock, N. W.; Busch, D. H.; Heppert, J. A. Copper(II) Template Synthesis of a 20-Membered [1 + 1] Schiff Base Macrocyclic and Nickel(II) Template Synthesis of a 40-Membered [2 + 2] Schiff Base Macrocyclic from 2,6-Pyridinedicarboxaldehyde and 1,13-Diamino-4,7,10-trioxatridecane. *Inorg. Chem.* **1997**, *36* (22), 5132–5134.
- (31) Garza-Ortiz, A.; Maheswari, P. U.; Siegler, M.; Spek, A. L.; Reedijk, J. Ruthenium(III) Chloride Complex with a Tridentate Bis(arylimino)pyridine Ligand: Synthesis, Spectra, X-ray Structure, 9-Ethylguanine Binding Pattern, and *In Vitro* Cytotoxicity. *Inorg. Chem.* **2008**, *47* (15), 6964–6973.
- (32) Luescher, M. U.; Vo, C. V.; Bode, J. W. SnAP Reagents for the Synthesis of Piperazines and Morpholines. *Org. Lett.* **2014**, *16* (4), 1236–1239.
- (33) Johnson, M. R.; Thelin, W. R.; Aungst, R. A. Dithiol Mucolytic Agents. U.S. Patent 14/458898, 2015.
- (34) Polt, R.; Kelly, B. D.; Dangel, B. D.; Tadikonda, U. B.; Ross, R. E.; Raitsimring, A. M.; Astashkin, A. V. Optically Active 4- and 5-Coordinate Transition Metal Complexes of Bifurcated Dipeptide Schiff Bases. *Inorg. Chem.* **2003**, *42* (2), S66–S74.
- (35) Chan, W. C.; White, P. D. *Fmoc Solid Phase Peptide Synthesis: a Practical Approach*; Oxford University Press: New York, 2000; pp xxiv, 346.
- (36) Manov, G. G.; DeLollis, N. J.; Acree, S. F. Comparative Liquid-Junction Potentials of Some pH Buffer Standards and the Calibration of pH Meters. *Journal of Research of the National Bureau of Standards (United States)* **1945**, *34*, 115–127 (Research Paper 1632).
- (37) Manov, G.G.; DeLollis, S.F.; DeLollis, S.F.; Lindvall, N.J.; Acree, P.W. Effect of Sodium Chloride on the Apparent Ionization Constant of Boric Acid and the pH Values of Borate Solutions. *Journal of Research of the National Bureau of Standards (United States)* **1946**, *36*, 543–558 (Research Paper 1721).
- (38) Irving, H. M.; Miles, M. G.; Pettit, L. D. A Study of Some Problems in Determining the Stoichiometric Proton Dissociation Constants of Complexes by Potentiometric Titrations Using a Glass Electrode. *Anal. Chim. Acta* **1967**, *38* (4), 475–88.
- (39) Zekany, L.; Nagypal, I. PSEQUAD. In *Computational Methods for the Determination of Formation Constants*; Leggett, D. J., Ed.; Springer: Boston, MA, 1985; pp 291–353.
- (40) Meiboom, S.; Gill, D. Modified Spin-Echo Method for Measuring Nuclear Relaxation Times. *Rev. Sci. Instrum.* **1958**, *29*, 688–691.

- (41) Raiford, D. S.; Fisk, C. L.; Becker, E. D. Calibration of Methanol and Ethylene Glycol Nuclear Magnetic Resonance Thermometers. *Anal. Chem.* **1979**, *51* (12), 2050–2051.
- (42) Micskei, K.; Helm, L.; Brucher, E.; Merbach, A. E. ^{17}O NMR Study of Water Exchange on $[\text{Gd}(\text{DTPA})(\text{H}_2\text{O})]^{2-}$ and $[\text{Gd}(\text{DOTA})(\text{H}_2\text{O})]^-$ Related to NMR imaging. *Inorg. Chem.* **1993**, *32* (18), 3844–3850.
- (43) Bonadio, F.; Senna, M. C.; Enslin, J.; Sieber, A.; Neels, A.; Stoeckli-Evans, H.; Decurtins, S. Cyano-Bridged Structures Based on $[\text{Mn}^{\text{II}}(\text{N}_3\text{O}_2\text{-Macrocycle})]^{2+}$: A Synthetic, Structural, and Magnetic Study. *Inorg. Chem.* **2005**, *44* (4), 969–978.
- (44) Richards, S.; Pedersen, B.; Silverton, J. V.; Hoard, J. D. Stereochemistry of Ethylenediaminetetraacetato Complexes. I. The Structure of Crystalline $\text{Mn}_3(\text{HY})_2 \cdot 10\text{H}_2\text{O}$ and the Configuration of the Seven-Coordinate $\text{Mn}(\text{OH}_2)\text{Y}^{2-}$ Ion. *Inorg. Chem.* **1964**, *3* (1), 27–33.
- (45) Liu, G.-F.; Filipovic, M.; Heinemann, F. W.; Ivanovic-Burmazovic, I. Seven-Coordinate Iron and Manganese Complexes with Acyclic and Rigid Pentadentate Chelates and Their Superoxide Dismutase Activity. *Inorg. Chem.* **2007**, *46* (21), 8825–8835.
- (46) Riley, D. P.; Weiss, R. H. Manganese Macrocylic Ligand Complexes as Mimics of Superoxide Dismutase. *J. Am. Chem. Soc.* **1994**, *116* (1), 387–388.
- (47) Neumann, W. L.; Franklin, G. W.; Sample, K. R.; Aston, K. W.; Weiss, R. H.; Riley, D. P. Synthesis of Conformationally Tailored Pentazacyclopentadecanes. Preorganizing Peptide Cyclizations. *Tetrahedron Lett.* **1997**, *38* (5), 779–782.
- (48) Hancock, R. D.; Bhavan, R.; Wade, P. W.; Boeyens, J. C. A.; Dobson, S. M. Ligand Design for Complexation in Aqueous Solution. 1. Neutral Oxygen Donor Bearing Groups as a Means of Controlling Size-Based Selectivity for Metal Ions. *Inorg. Chem.* **1989**, *28* (2), 187–194.
- (49) Cabral, M. F.; Delgado, R. Metal Complexes of Pentadentate Macrocylic Ligands Containing Oxygen and Nitrogen as Donor Atoms. *Helv. Chim. Acta* **1994**, *77* (2), 515–524.
- (50) Irving, H.; Williams, R. J. P. The Stability of Transition-metal Complexes. *J. Chem. Soc.* **1953**, 3192–3210.
- (51) Rossiter, C. S.; Mathews, R. A.; Morrow, J. R. Uridine Binding by $\text{Zn}(\text{II})$ Macrocylic Complexes: Diversion of RNA Cleavage Catalysts. *Inorg. Chem.* **2005**, *44* (25), 9397–9404.
- (52) Gale, E. M.; Zhu, J.; Caravan, P. Direct Measurement of the $\text{Mn}(\text{II})$ Hydration State in Metal Complexes and Metalloproteins Through ^{17}O NMR Line Widths. *J. Am. Chem. Soc.* **2013**, *135* (49), 18600–18608.
- (53) Rohrer, M.; Bauer, H.; Mintonovitch, J.; Requardt, M.; Weinmann, H.-J. Comparison of Magnetic Properties of MRI Contrast Media Solutions at Different Magnetic Field Strengths. *Invest. Radiol.* **2005**, *40* (11), 715–724.
- (54) Swift, T. J.; Connick, R. E. NMR-Relaxation Mechanisms of ^{17}O in Aqueous Solutions of Paramagnetic Cations and the Lifetime of Water Molecules in the First Coordination Sphere. *J. Chem. Phys.* **1962**, *37* (2), 307–320.
- (55) Swift, T. J.; Connick, R. E. Erratum: NMR-Relaxation Mechanisms of ^{17}O in Aqueous Solutions of Paramagnetic Cations and the Lifetime of Water Molecules in the First Coordination Sphere. *J. Chem. Phys.* **1964**, *41* (8), 2553–2554.
- (56) Balogh, E.; He, Z.; Hsieh, W.; Liu, S.; Tóth, É. Dinuclear Complexes Formed with the Triazacyclononane Derivative ENOTA⁺: High-Pressure ^{17}O NMR Evidence of an Associative Water Exchange on $[\text{Mn}^{\text{II}}(\text{ENOTA})(\text{H}_2\text{O})_2]$. *Inorg. Chem.* **2007**, *46* (1), 238–250.
- (57) Vanasschen, C.; Molnár, E.; Tircsó, G.; Kálmán, F. K.; Tóth, E. v.; Brandt, M.; Coenen, H. H.; Neumaier, B. Novel CDTA-based, Bifunctional Chelators for Stable and Inert Mn^{II} Complexation: Synthesis and Physicochemical Characterization. *Inorg. Chem.* **2017**, *56* (14), 7746–7760.
- (58) Freire, D. M.; Beerli, D.; Pota, K.; Johnston, H. M.; Palacios, P.; Pierce, B. S.; Sherman, B. D.; Green, K. N. Hydrogen Peroxide Disproportionation with Manganese Macrocylic Complexes of Cyclen and Pycen. *Inorg. Chem. Front.* **2020**, *7* (7), 1573–1582.